Cogging torque definitions for magnetic gears and magnetically geared electrical machines (repository copy)

Article:
Gerber, S., Wang, R-J., (2018) Cogging torque definitions of magnetic gears and magnetically geared machines. IEEE Transactions on Magnetics, 54(4): 8103209, April 2018; ISSN: 1941-0069

https://doi.org/10.1109/TMAG.2017.2784823

Cogging Torque Definitions for Magnetic Gears and Magnetically Geared Electrical Machines

Stiaan Gerber and Rong-Jie Wang

Department of Electrical and Electronic Engineering, Stellenbosch University, Stellenbosch 7600, South Africa

Although cogging torque in magnetic gears (MGs) has been studied, the additional degree of freedom inherent to MGs makes it unclear exactly what is defined as the cogging torque of a MG. Although MGs generally have relatively smooth torque transfer characteristics, this paper reveals that when the gear is used in an up-speed configuration, cogging effects may be amplified under startup conditions. This paper distinguishes between two kinds of cogging torque in MGs, termed the *synchronous cogging torque* and the *true cogging torque*. Calculation of the true cogging torque is more difficult than the synchronous cogging torque, but an approximation to the true cogging torque can be obtained using the synchronous cogging torque. The theory is verified experimentally and supported further by results from dynamic simulations. The impact on magnetically geared machines is also considered.

***Index Terms*— Cogging torque, dynamic modeling, magnetic gears (MGs).**

I. Introduction

MAGNETIC gears have received much attention in recent years. Several torque dense magnetic gear (MG) technologies, such as harmonic, flux modulated, and planetary MGs, have been proposed in the literature [1]–[4]. Among them, the flux modulated MG attracts the most interest because of its less complex mechanical structure and the ease of integrating an MG and an electrical machine in a single volume [5], [6].

As shown in Fig. 1, an MG consists of three concentric components, namely, an outer magnet assembly with high pole count, a flux modulator, and an inner magnet assembly with low pole count. Similar to any conventional permanent magnet (PM) machine with a slotted stator, the MGs are also prone to cogging/ripple torques due to the slotting effects of the modulator. Studies on cogging torques and their mitigation measures can be found in the literature. In [7], a cogging torque factor originally derived as a guidance for the judicious selection of pole–slot combination in conventional PM machines was first applied for MG designs, which shows that the lowest cogging factor is associated with fractional gear ratios as also explained in [8] and [9]. However, considering the unbalanced magnetic forces generated inside a MG, the pole–slot combinations with the lowest cogging factors are usually not preferred [19]. A detailed analysis of cogging torque composition of an MG was conducted in [10]. Cogging torque reduction techniques, such as step [11] or continuous [12] skewing of the complete MG, step [13] or continuous [14] skewing of inner magnet assembly, and pole-pairing of both inner and outer magnet assemblies [15], [16], were also proposed in the literature.

Manuscript received August 8, 2017; revised October 27, 2017; accepted December 5, 2017. Date of publication February 21, 2018; date of current version March 16, 2018. Corresponding author: S. Gerber (e-mail: sgerber@sun.ac.za).

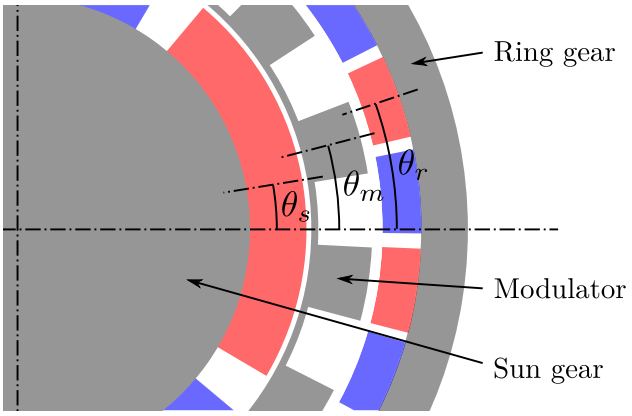

Fig. 1. MG component names and positions.

Unlike conventional PM machines, the magnetic field interactions among three concentric components of an MG are inherently more complex. The distinct difference in the mechanism of cogging torque generation between an MG and a conventional PM machine has not been well described in the literature. Cogging torques are undesirable torque components and may adversely affect the operating performance of an MG. For example, in the wind power industry, gearboxes are often used for up-speed applications. Given the relatively low developed torque of wind turbines under startup conditions, high cogging torque in an MG may result in complete failure of starting up.

This paper attempts to provide a better understanding of the cogging torque mechanism in an MG and devise a computation method for accurately predicting the cogging torque under different operating conditions. In Section II, the terminology used in this paper is discussed briefly. The theoretical aspects are presented in Section III and supported by dynamic modeling in Section IV. Then, the impact on magnetically geared machines (MGMs) is considered in Section V and thereafter, conclusions are drawn.

II. Magnetic Gear Nomenclature

In this paper, the three components comprising a MG are referred to as the sun gear, modulator, and ring gear. The notations used to describe the angular position of the three components are shown in Fig. 1, where θ_s, θ_m, and θ_r represent the positions of the sun gear, modulator, and ring gear, respectively. The sun and ring gear positions are measured between the datum and the center of poles of the same polarity. The modulator position is measured between the datum and the center of a modulator segment. The position of the datum is arbitrary.

The torque on the three components of the MG can be expressed as a sinusoidal function of the MGs load angle [17]. The load angle is defined as

$$\delta = p_s\theta_s + p_r\theta_r - Q_m\theta_m \tag{1}$$

where p_s is the number of sun gear pole pairs, p_r is the number of ring gear pole pairs, and Q_m is the number of modulator segments. The average torque on the components is then

$$T_s^{\text{avg}} = -T_s' \sin\delta \tag{2}$$
$$T_r^{\text{avg}} = -T_r' \sin\delta \tag{3}$$
$$T_m^{\text{avg}} = T_m' \sin\delta \tag{4}$$

where the prime superscripts indicate stall torque magnitudes.

III. Cogging Torque Definitions

Cogging torque in PM machines has been studied extensively. PM machines have one degree of freedom, which leads to a simple definition of cogging torque. MGs, on the other hand, have two degrees of freedom, since the high- and low-speed components can rotate independently. Because of the additional degree of freedom, the definition of cogging torque in a MG is not as clear as in PM machines. This fact has not been well recognized in the literature thus far. In this section, two different definitions of cogging torque in MGs are proposed and the importance of both definitions is highlighted.

During the discussion, we will consider two MGs designs with cross sections as shown in Fig. 2. A prototype of Design A was realized and used for experimental verification. The gears' design parameters are listed in Table I. We will consider the mode of operation where the ring gear is held stationary and the sun gear and the modulator act as high- and low-speed components, respectively, but the theory presented here is just as applicable to other modes of operation.

Since MGs with one stationary component have two degrees of freedom, their torque characteristics can be represented by surface plots. In our case where the ring gear is stationary, the independent variables can be any two of θ_s, θ_m and δ. The other dependent variable is determined from (1). For example, contour plots of the torque on the sun gear and the modulator versus the modulator position and the load angle are shown in Figs. 3 and 4 for Designs A and B, respectively. These maps were obtained using static finite element analyses, where the rotor positions were systematically varied over the displayed range. In these figures, we have plotted $T_s(\theta_m, \delta)$ and

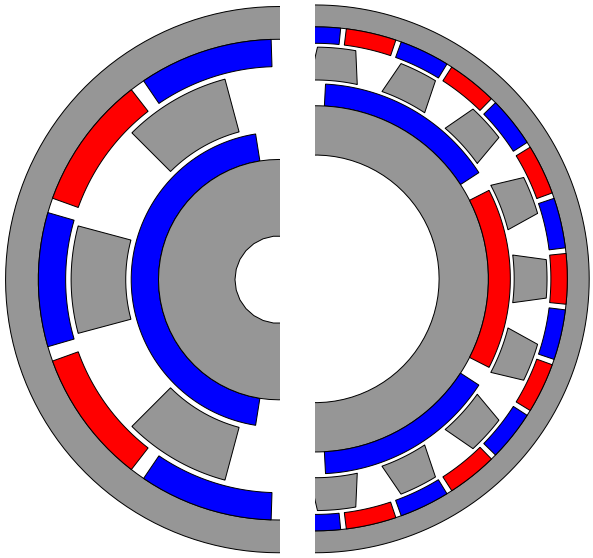

Fig. 2. Cross-sectional views of two MG designs. (a) Design A. (b) Design B.

TABLE I
MG Design Parameters

Parameter	Design A	Design B
Sun gear pole pairs, p_s	1	3
Modulator segments, Q_m	6	17
Ring gear pole pairs, p_r	5	14
Sun gear magnet pitch/pole pitch	0.9	0.9
Inner modulator tooth pitch/segment pitch	0.5	0.65
Outer modulator tooth pitch/segment pitch	0.5	0.45
Ring gear magnet pitch/pole pitch	0.9	0.9
Outer radius	50 mm	50 mm
Ring gear yoke thickness	6 mm	4 mm
Ring gear magnet thickness	5 mm	3 mm
Ring gear air-gap length	1 mm	0.7 mm
Modulator thickness	10 mm	6 mm
Sun gear air-gap length	1 mm	0.7 mm
Sun gear magnet thickness	5 mm	4 mm
Sun gear yoke thickness	14 mm	9 mm
Stack length	30 mm	30 mm
Magnet remanence	1.195 T	1.195 T
Magnet relative recoil permeability	1.049	1.049

$T_m(\theta_m, \delta)$; however, the torques T_s and T_m can be expressed as functions of any two of the variables θ_s, θ_m, and δ by changing variables according to (1). As can be seen in Fig. 3, the torque on the components are dependent not only on the load angle, as in (2)–(4), but also on the component positions. These torque variations are due to cogging effects. Design A clearly suffers from large cogging effects. In Fig. 4, the torque on the components of Design B show very little variation with component position due to this design's smooth torque transfer characteristics.

By subtracting the average torques given by (2) and (4) from the torques $T_s(\theta_s, \delta)$ and $T_m(\theta_m, \delta)$, the cogging torque as a function of position and load angle can be obtained

$$T_s^C(\theta_s, \delta) = T_s(\theta_s, \delta) + T_s' \sin\delta \tag{5}$$
$$T_m^C(\theta_m, \delta) = T_m(\theta_m, \delta) - T_m' \sin\delta. \tag{6}$$

The cogging torque maps of Design A are shown in Fig. 5. Although maps such as these give a lot of information about

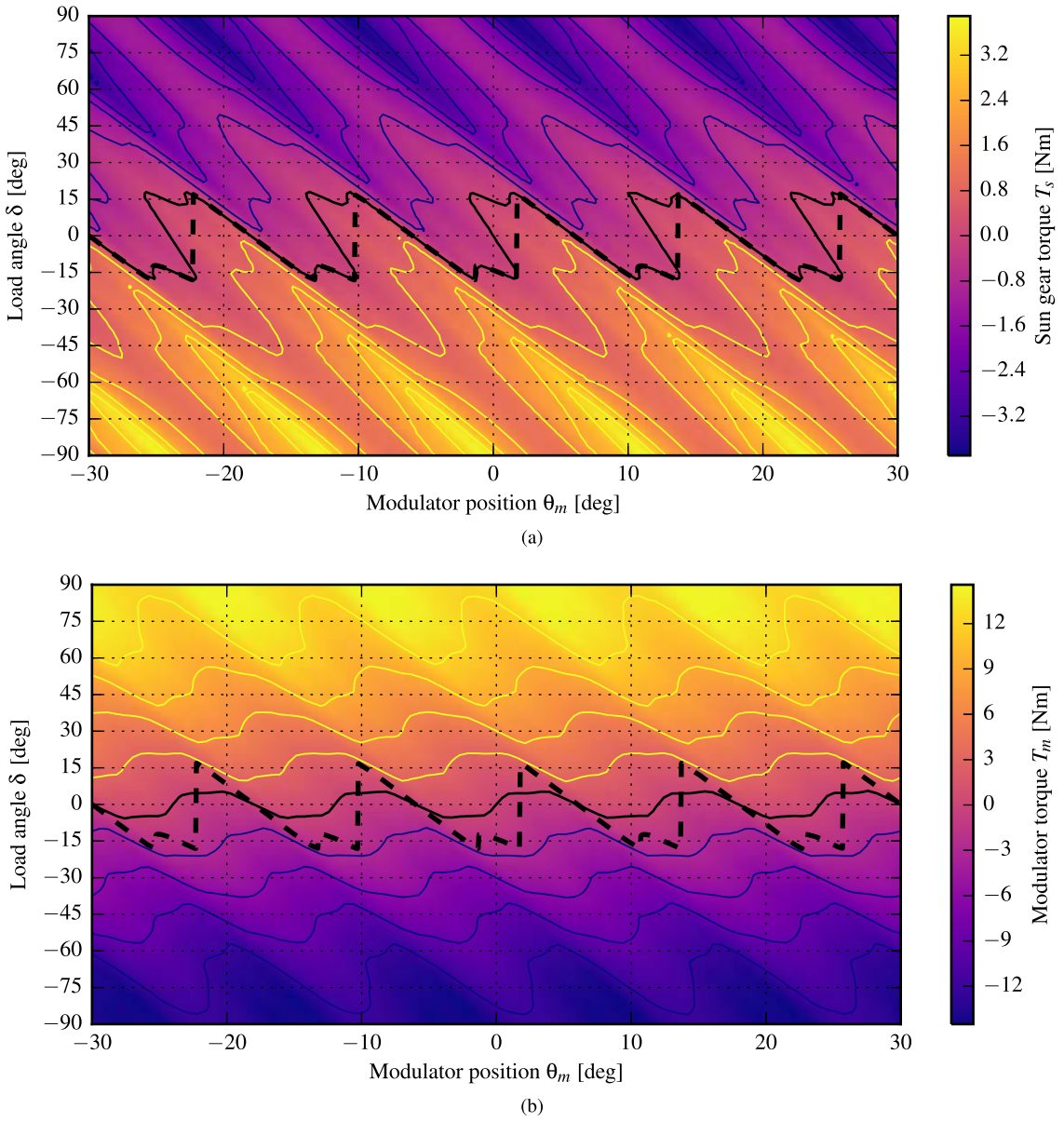

Fig. 3. Torque maps versus position and load angle for Design A. (a) Sun gear torque. (b) Modulator torque.

the cogging behavior of MGs, it still does not fully describe the impact of cogging effects on the dynamic performance of MGs. In order to give more practical measures of torque performance, we have defined two kinds of cogging torque.

A. Synchronous Cogging Torque

The first kind of cogging torque is referred to as the *synchronous cogging torque*. It is defined as the torque on a component of the MG when the MGs load angle is zero

$$T_s^{\text{sync}}(\theta_s) = T_s(\theta_s, \delta = 0) \tag{7}$$

$$T_m^{\text{sync}}(\theta_m) = T_m(\theta_m, \delta = 0). \tag{8}$$

Referring to Figs. 3–5, the synchronous cogging torque is evaluated along the horizontal lines $\delta = 0$. Along these lines, the gear operates at no-load, as the average torques from (2)–(4) are zero. When the MG torque is evaluated at constant but nonzero load angles, the resulting torque may be referred to as the *synchronous torque ripple*.

In most publications dealing with cogging torque in MGs, it is the synchronous cogging torque or torque ripple that has been considered [8]–[16]. The synchronous cogging torque is an accurate representation of the no-load torque ripple when the inertias of the rotating components are large enough to prevent significant oscillations in the gear's load angle due to cogging effects, as will be demonstrated in Section IV.

B. True Cogging Torque

In some applications, including many renewable energy applications, gearboxes are used as a means of increasing the speed and reducing the torque provided by a prime mover.

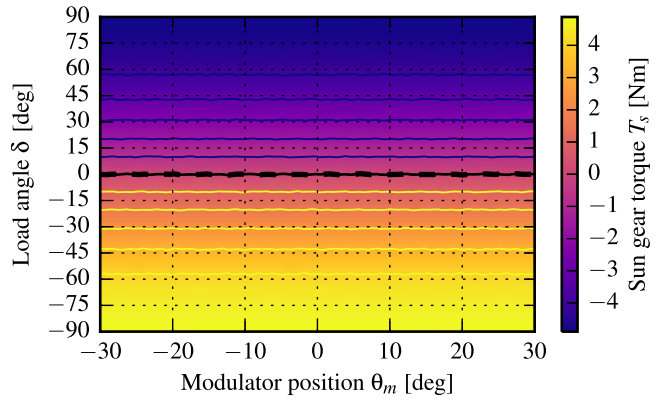

Fig. 4. Torque maps versus position and load angle for Design B. (a) Sun gear torque. (b) Modulator torque.

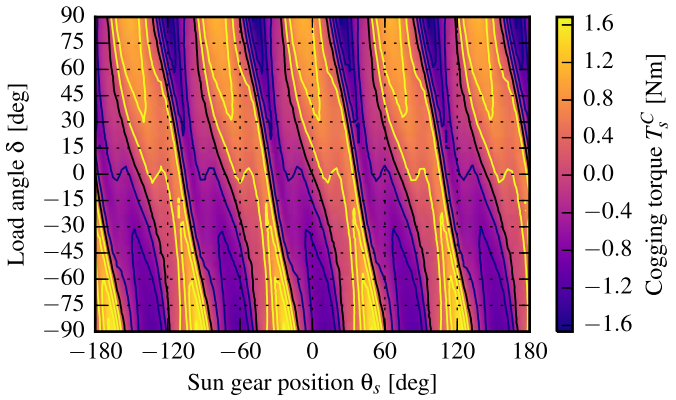

Fig. 5. Cogging torque maps versus position and load angle. (a) Sun gear cogging torque. (b) Modulator cogging torque.

Under startup conditions, the rotating components of a MG are not moving fast enough for oscillations in load angle to be insignificant. When one rotor is moved, the other will naturally seek its equilibrium position. The true cogging torque on a component is defined as the torque on the component when other components are at their equilibrium positions

$$T_s^{\text{true}}(\theta_s) = T_s\big(\theta_s, \delta_m^*(\theta_s)\big) \tag{9}$$
$$T_m^{\text{true}}(\theta_m) = T_m\big(\theta_m, \delta_s^*(\theta_m)\big) \tag{10}$$

where $\delta_s^*(\theta_m)$ and $\delta_m^*(\theta_s)$ are the load angles at which the sun gear and the modulator, respectively, are at equilibrium. The load angles can be found by solving the following equations:

$$T_m\big(\theta_s, \delta_m^*\big) = 0 \tag{11}$$
$$T_s\big(\theta_m, \delta_s^*\big) = 0. \tag{12}$$

For example, the solution of (12) is represented by the dashed line in Fig. 3(a). The true cogging torque, given by (10), is then evaluated along this dashed line, as shown in Fig. 3(b).

C. Comparison of Cogging Torques

The different cogging torques have been calculated for the two designs of Fig. 2. Waveforms for Designs A and B are shown in Figs. 6 and 7, respectively. Importantly, the true cogging torque on the modulator is much larger than the synchronous cogging torque in both cases. It is the peak value of the true cogging torque that has to be overcome in up-speed configurations for the system to start successfully.

D. True Cogging Torque Approximation

Calculation of the true cogging torque is not as straightforward as calculating the synchronous cogging torque because the load angles δ_m^* and δ_s^* have to be found by solving (11) and (12). This requires more evaluations of the torque for different component positions compared to that required for calculating the synchronous cogging torque where δ is known. However, it will be shown that an approximation to the true cogging torque can be found, given the synchronous cogging torque.

In this derivation, it is assumed that the torque on a component can be expressed by a superposition of the synchronous cogging torque and (2) or (4), such that

$$T_s(\theta_s, \delta) = T_s^{\text{sync}}(\theta_s) - T_s' \sin\delta \tag{13}$$
$$T_s(\theta_m, \delta) = T_s^{\text{sync}}(\theta_m) - T_s' \sin\delta \tag{14}$$
$$T_m(\theta_s, \delta) = T_m^{\text{sync}}(\theta_s) + T_m' \sin\delta \tag{15}$$
$$T_m(\theta_m, \delta) = T_m^{\text{sync}}(\theta_m) + T_m' \sin\delta. \tag{16}$$

While the above assumptions do introduce errors, it will be shown that useful approximations can be produced

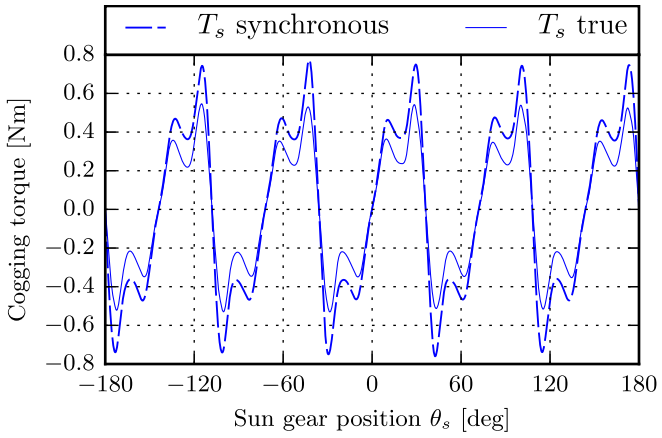

(a)

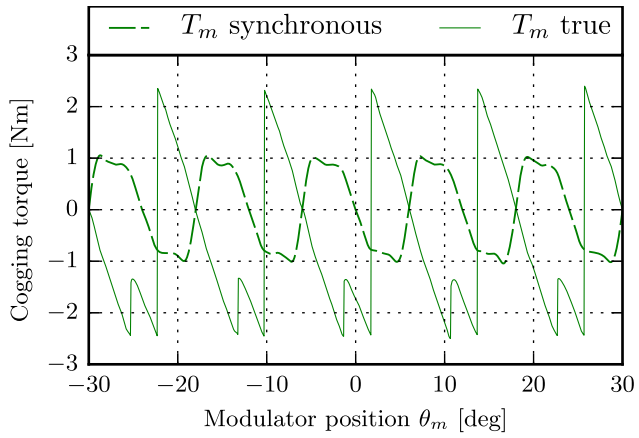

(b)

Fig. 6. Comparison of different cogging torque waveforms of Design A. (a) Sun gear cogging torques. (b) Modulator cogging torques.

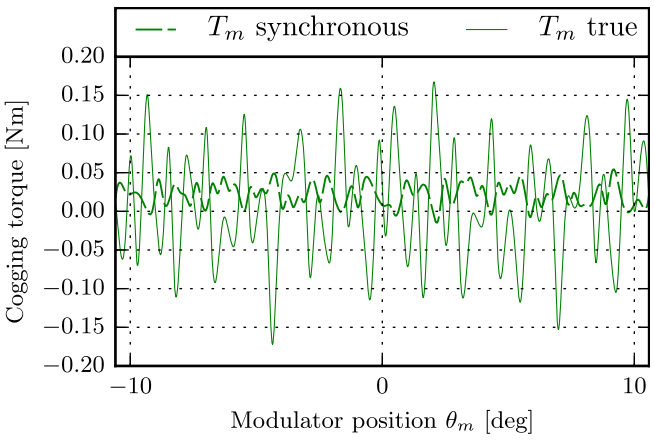

Fig. 7. Comparison of different modulator cogging torque waveforms for Design B.

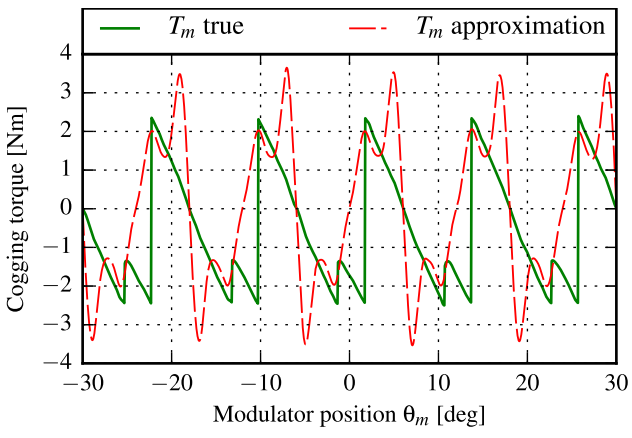

(a)

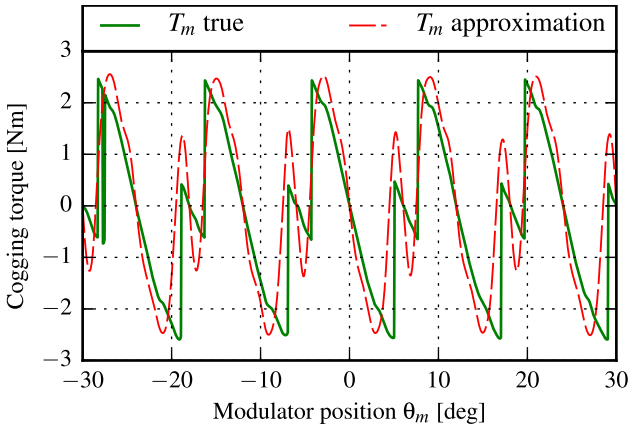

(b)

Fig. 8. Approximation to the modulator true cogging torque obtained from the synchronous cogging torque for Design A. (a) Nonlinear BH curve. (b) Linear BH curve.

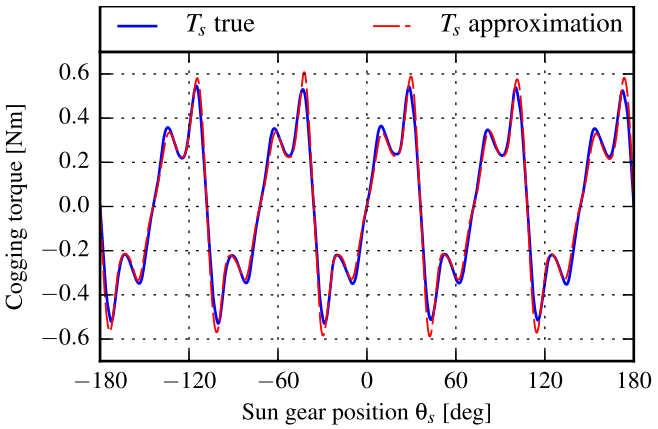

Fig. 9. Approximation to the sun gear true cogging torque obtained from the synchronous cogging torque for Design A.

nonetheless. From (14) and (15), the equilibrium load angles angles can be found

$$T_s^{\text{sync}}(\theta_m) - T_s' \sin \delta_s^*(\theta_m) = 0 \tag{17}$$

$$\sin \delta_s^*(\theta_m) = \frac{T_s^{\text{sync}}(\theta_m)}{T_s'} \tag{18}$$

$$T_m^{\text{sync}}(\theta_s) + T_m' \sin \delta_m^*(\theta_s) = 0 \tag{19}$$

$$\sin \delta_m^*(\theta_s) = -\frac{T_m^{\text{sync}}(\theta_s)}{T_m'}. \tag{20}$$

Now, the true cogging torque can be evaluated by substituting the equilibrium load angles back, (20) into (13) and (18)

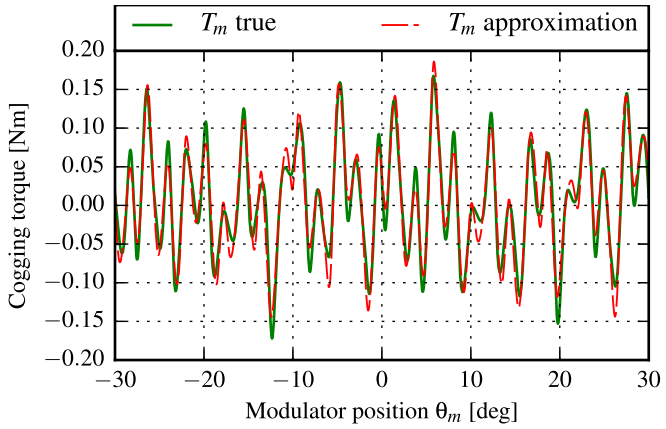

Fig. 10. Approximation to the modulator true cogging torque obtained from the synchronous cogging torque for Design B (nonlinear BH curve).

into (16)

$$T_s\left(\theta_s, \delta_m^*\right) = T_s^{\text{sync}}(\theta_s) + T_m^{\text{sync}}(\theta_s)\frac{T_s'}{T_m'} \tag{21}$$

$$T_m\left(\theta_m, \delta_s^*\right) = T_m^{\text{sync}}(\theta_m) + T_s^{\text{sync}}(\theta_m)\frac{T_m'}{T_s'}. \tag{22}$$

Recognizing that the ratio of the stall torques is equal to the gear ratio

$$\frac{T_m'}{T_s'} = \frac{Q_m}{p_s} \tag{23}$$

the expressions (21) and (22) can be further simplified, to finally obtain

$$T_s^{\text{true}}(\theta_s) \approx T_s^{\text{sync}}(\theta_s) + \frac{p_s}{Q_m}T_m^{\text{sync}}(\theta_s) \tag{24}$$

$$T_m^{\text{true}}(\theta_m) \approx T_m^{\text{sync}}(\theta_m) + \frac{Q_m}{p_s}T_s^{\text{sync}}(\theta_m). \tag{25}$$

Figs. 8 and 9 show comparisons of true cogging torque waveforms for Design A obtained using the exact method and the approximation (25). In the case of this design, the approximation does not predict the modulator true cogging torque very accurately, as can be seen in Fig. 8(a). If the torque maps of this gear are calculated using linear BH curves, the resulting true cogging torque waveform and approximation are shown in Fig. 8(b). Here, the approximation gives a better prediction of the true cogging torque, but the waveform differs from that obtained using nonlinear solutions. A comparison of the exact and approximate modulator true cogging torques of Design B is shown in Fig. 10. For Design B, where the cogging effects are much less significant, the approximation gives an accurate prediction of the modulator true cogging torque even when considering nonlinear BH curves. Since Design B reflects the typical cogging behavior of MGs more closely than Design A, it can be concluded that the approximation can generally be used as an accurate prediction of true cogging torque.

E. Experimental Verification

The peak value of the true cogging torque of the prototype of Design A was measured using the experimental setup shown in Fig. 11. A torque sensor was mounted on the input side of the MG with no load connected on the output. The gear was then slowly rotated and the peak torque value, which is the peak value of the true cogging torque, was observed. This procedure was used to measure the true cogging torque of the sun gear and the modulator. Several measurements were taken for each case. The measured waveforms are overlaid in Figs. 12 and 13.

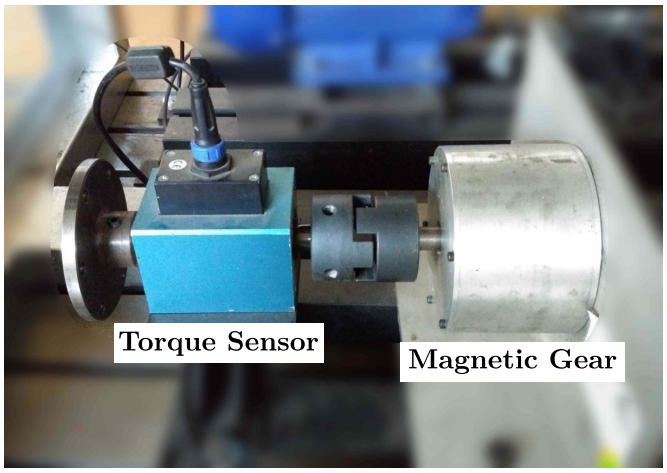

Fig. 11. Experimental setup used to measure peak values of the true cogging torque.

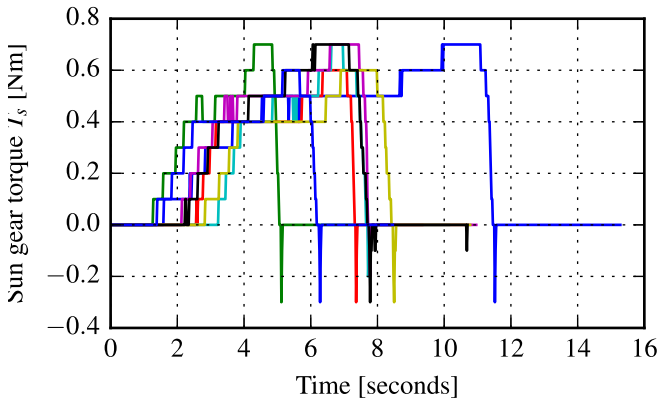

Fig. 12. Measurements of the peak value of the true cogging torque of the sun gear.

The lowest recorded peak values of the torque on the sun gear and the modulator were 0.6 and 4.9 Nm, respectively. The simulated values were 0.54 and 2.50 Nm, respectively. Although the measured value of the true cogging torque of the modulator does not match the simulated result closely, its large magnitude confirms the theory to some extent. The discrepancy in this result may be attributed to the modulator construction, where the segments were inter-connected by a mild steel ring, and other manufacturing imperfections. In addition, the modulator true cogging torque also reflects any frictional torque on the sun gear amplified by the gear ratio, according to (25).

Table II summarizes the findings. The simulated and measured results clearly indicate the importance of considering the true cogging torque in up-speed configurations.

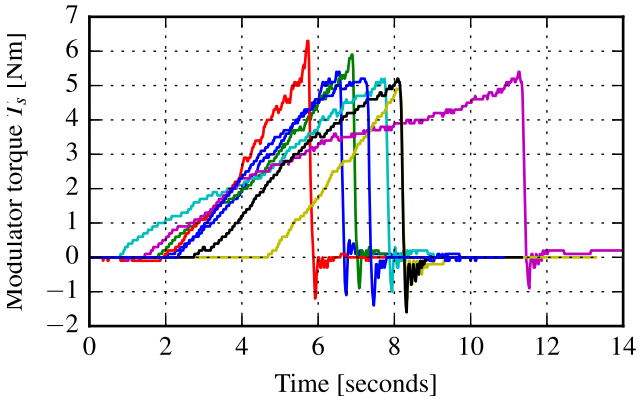

Fig. 13. Measurements of the peak value of the true cogging torque of the modulator.

TABLE II
MG: RESULTS

Parameter	Design A Simulated		Design A Measured		Design B Simulated	
	[Nm]	[%]	[Nm]	[%]	[Nm]	[%]
T_s'	2.23	100	2.4	107.6	4.85	100
T_m'	13.36	100	8.9	66.6	27.49	100
T_s^{sync}	0.77	34.45	-	-	0.033	0.671
T_m^{sync}	1.05	7.87	-	-	0.035	0.126
T_s^{true}	0.54	24.19	0.6	26.9	0.028	0.575
T_m^{true}	2.50	18.72	4.9	36.7	0.172	0.627

IV. Dynamic Cogging Torque Simulations

In order to further illustrate the different cogging torque behaviors, dynamic simulations have been conducted on Design A. The MG model is defined by the following equations:

$$T_s(\theta_s, \delta) = I_s\ddot{\theta}_s + B_s\dot{\theta}_s + T_{sL} \quad (26)$$

$$T_m(\theta_m, \delta) = I_m\ddot{\theta}_m + B_m\dot{\theta}_m + T_{mL} \quad (27)$$

where I_s and I_m are the sun gear and modulator moments of inertia, B_s and B_m are rotational damping coefficients and T_{sL} and T_{mL} are the load torques applied to the sun gear and modulator, respectively. The sun gear and modulator dynamics, (26) and (27), are coupled by the load angle δ given by (1). The functions $T_s(\theta_s, \delta)$ and $T_m(\theta_m, \delta)$ were implemented using a linearly interpolated lookup table of the data generated by finite element simulations, as displayed in Fig. 3.

A. Synchronous Cogging Dynamics

The MG was simulated operating at high speed with large dead load inertias attached to the sun gear and the modulator. Fig. 14 shows the variation in the MGs load angle and the torque on the sun gear and the modulator under these operating conditions. As expected, in this scenario, the torque waveforms resemble the synchronous cogging torque waveforms.

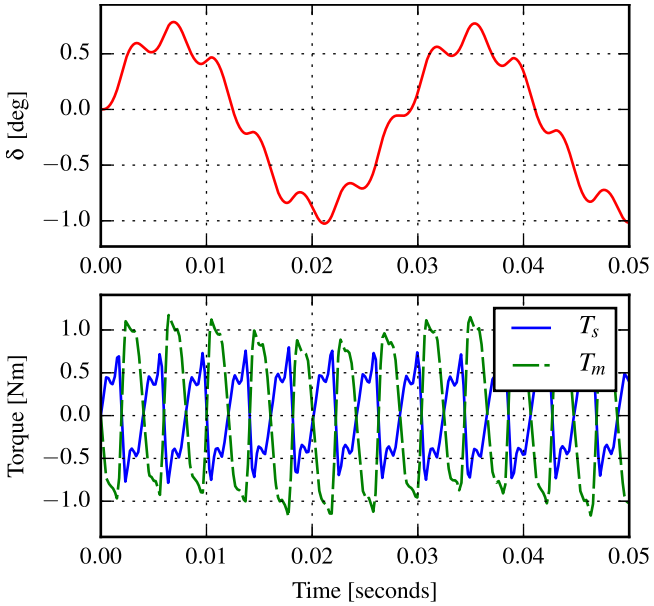

Fig. 14. Dynamic behavior under high-speed operation with large inertias connected to the gear.

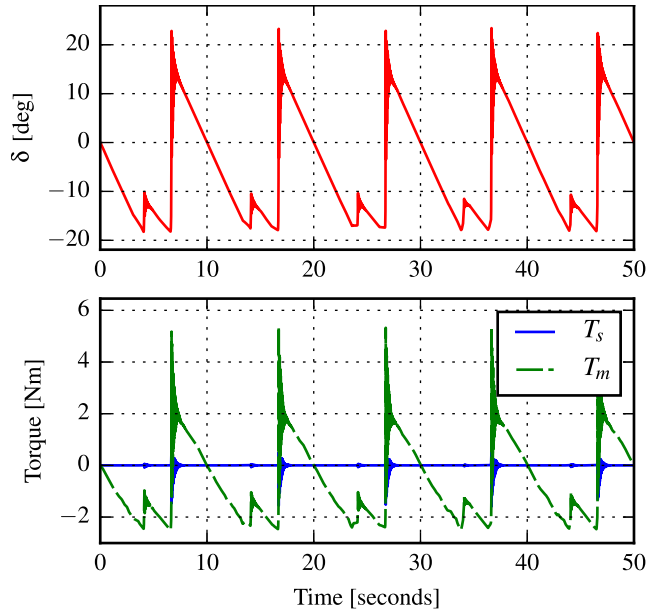

Fig. 15. Dynamic behavior under slow rotation of the modulator.

B. True Cogging Dynamics

A second simulation was conducted where the modulator was driven at a constant low speed and no additional load was placed on the sun gear. Fig. 15 shows the behavior of the gear in this scenario. Note that the amplitude of the torque on the modulator is much larger than in the case of the previous scenario and that the peak value agrees with that of the true cogging torque.

V. Impact on Magnetically Geared Machines

It may be even more vital to consider the true cogging torque in MGMs used as generators where starting

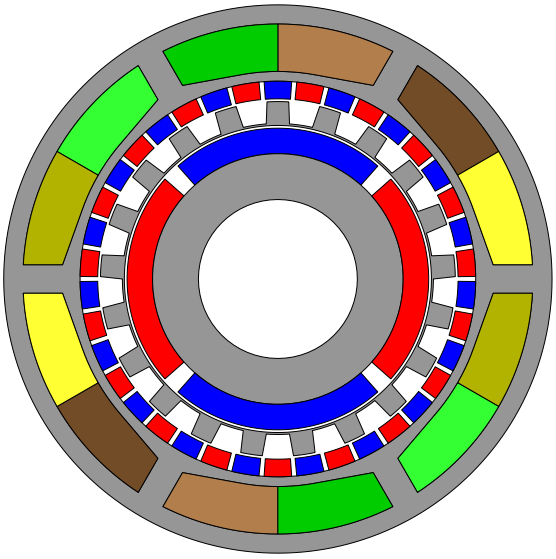

Fig. 16. Cross-sectional view of a MGM with an outer stator.

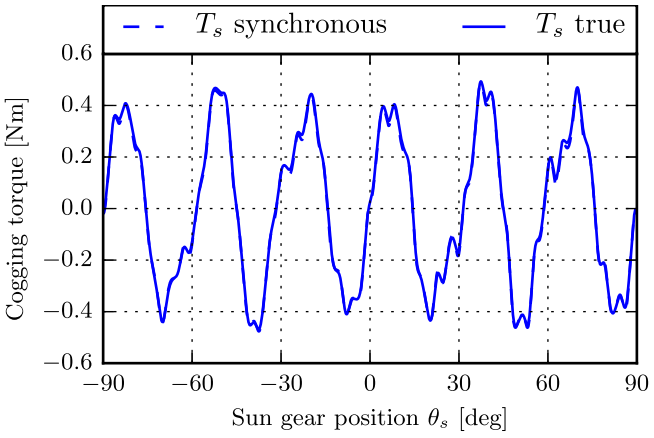

(a)

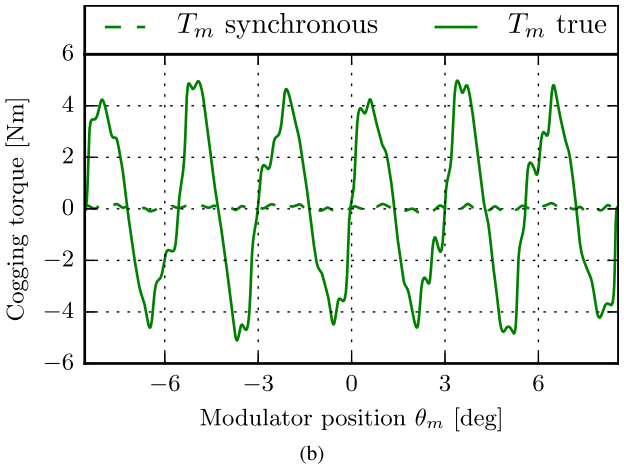

(b)

Fig. 17. Comparison of different cogging torque waveforms for the MGM of Fig. 16. (a) Sun gear cogging torques. (b) Modulator cogging torques.

performance is important. Applications such as wind power generation fall in this category. In MGMs, the interaction between the sun gear and the stator teeth is an additional source of cogging effects. From (25), it can be seen that the

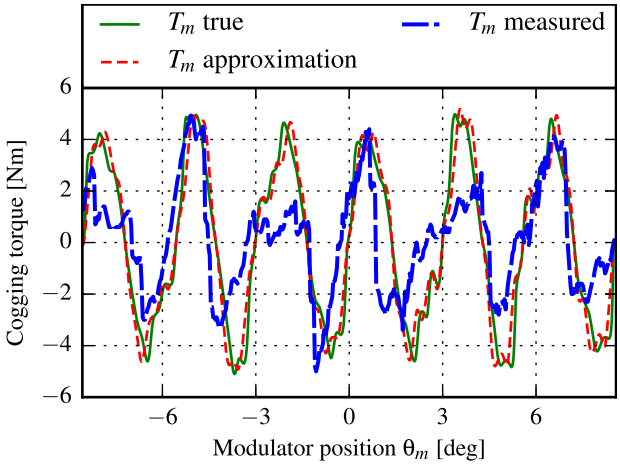

Fig. 18. Comparison of calculated true cogging, the approximation (25), and measured data for the MGM of Fig. 16.

TABLE III
MGM: RESULTS

Parameter	Simulated		Measured	
	[Nm]	[%]	[Nm]	[%]
T_s'	7.20	100	-	-
T_m'	75.7	100	59	77.9
T_s^{sync}	0.483	6.71	-	-
T_m^{sync}	0.174	0.23	-	-
T_s^{true}	0.481	6.68	-	-
T_m^{true}	4.98	6.58	∼4	5.28

true cogging torque on the modulator contains an amplified version of the sun gear synchronous cogging torque. Thus, in these applications it is very important to minimize the cogging effects resulting from the sun gear's interaction with the stator. Furthermore, the sun gear is not connected to any load that adds additional inertia to the sun gear. This allows load angle oscillations to occur relatively easily.

Fig. 16 shows a cross section of an MGM that was designed in a previous study [18]. The cogging torques described in Section III were also calculated for this machine to demonstrate the difference between the synchronous cogging torque and the true cogging torque in MGMs. Fig. 17 shows a comparison of the various cogging torque waveforms. Again, it is clear that the true cogging torque on the modulator resembles an amplified version of the synchronous cogging torque on the sun gear.

The approximation (25) can also be applied to MGMs. Fig. 18 compares the true cogging torque calculated using the exact method and the approximation with measured data. The measured waveform was obtained by loading the sun gear with a counterweight and sampling the modulator torque at different positions. The cogging torque was then extracted by subtracting the average torque resulting from the counterweight. Fig. 18 shows that the peak-to-peak amplitude is estimated accurately using both calculation methods. The results are summarized in Table III.

VI. Conclusion

Although it is generally not difficult to design MGs that have smooth torque transfer characteristics when the load angle is constant, this paper has highlighted the importance of considering load angle fluctuations in some applications. In up-speed configurations under startup conditions, these effects are especially important.

A clear distinction has been made between the *synchronous cogging torque* which applies when the load angle is constant and the *true cogging torque* which is relevant when load angle fluctuations can occur freely. It has been shown that the true cogging torque on the low-speed side is dominated by an amplified version of the synchronous cogging torque on the high-speed side.

The two types of cogging torque are also important in MGMs, especially ones operating as generators.

Acknowledgment

This work was supported in part by the ABB Corporate Research, Sweden, and in part by the National Research Foundation of South Africa.

References

[1] K. Atallah and D. Howe, "A novel high-performance magnetic gear," *IEEE Trans. Magn.*, vol. 37, no. 4, pp. 2844–2846, Jul. 2001.

[2] K. Davey *et al.*, "Rotating cylinder planetary gear motor," *IEEE Trans. Ind. Appl.*, vol. 52, no. 3, pp. 2253–2260, May 2016.

[3] C.-C. Huang, M.-C. Tsai, D. G. Dorrell, and B.-J. Lin, "Development of a magnetic planetary gearbox," *IEEE Trans. Magn.*, vol. 44, no. 3, pp. 403–412, Mar. 2008.

[4] J. Rens, K. Atallah, S. D. Calverley, and D. Howe, "A novel magnetic harmonic gear," in *Proc. IEEE Int. Electr. Mach. Drives Conf. (IEMDC)*, May 2007, pp. 698–703.

[5] P. M. Tlali, R.-J. Wang, and S. Gerber, "Magnetic gear technologies: A review," in *Proc. Int. Conf. Elect. Mach. (ICEM)*, Berlin, Germany, Sep. 2014, pp. 544–550.

[6] C. G. C. Neves, Á. F. Flores, D. L. Figueiredo, and A. S. Nunes, "Magnetic gear: A review," in *Proc. 11th IEEE/IAS Int. Conf. Ind. Appl. (INDUSCON)*, Juiz de Fora, Brazil, Dec. 2014, pp. 1–6.

[7] K. Atallah, S. D. Calverley, and D. Howe, "Design, analysis and realisation of a high-performance magnetic gear," *IEE Proc.-Electr. Power Appl.*, vol. 151, no. 2, pp. 135–143, Mar. 2004.

[8] N. W. Frank and H. A. Toliyat, "Gearing ratios of a magnetic gear for marine applications," in *Proc. IEEE Electr. Ship Technol. Symp. (ESTS)*, Apr. 2009, pp. 477–481.

[9] N. W. Frank and H. A. Toliyat, "Gearing ratios of a magnetic gear for wind turbines," in *Proc. IEEE Int. Electr. Mach. Drives Conf.*, May 2009, pp. 1224–1230.

[10] N. Niguchi and K. Hirata, "Cogging torque analysis of magnetic gear," *IEEE Trans. Ind. Electron.*, vol. 59, no. 5, pp. 2189–2197, May 2012.

[11] H. Zaytoon, A. S. Abdel-Khalik, S. Ahmed, and A. Massoud, "Torque ripple alleviation of a radial magnetic gearbox using step skewing approach," in *Proc. Int. Conf. Elect. Mach. (ICEM)*, Berlin, Germany, Sep. 2014, pp. 648–653.

[12] S. A. Afsari, H. Heydari, and B. Dianati, "Cogging torque mitigation in axial flux magnetic gear system based on skew effects using an improved quasi 3-D analytical method," *IEEE Trans. Magn.*, vol. 51, no. 9, Sep. 2015, Art. no. 7403111.

[13] N. Niguchi, K. Hirata, M. Muramatsu, and Y. Hayakawa, "Transmission torque characteristics in a magnetic gear," in *Proc. Int. Conf. Elect. Mach. (ICEM)*, Berlin, Germany, Sep. 2014, pp. 1–6.

[14] G. Jungmayr, J. Loeffler, B. Winter, F. Jeske, and W. Amrhein, "Magnetic gear: Radial force, cogging torque, skewing, and optimization," *IEEE Trans. Ind. Appl.*, vol. 52, no. 5, pp. 3822–3830, Sep. 2016.

[15] H. Zaytoon, A. S. Abdel-Khalik, A. Massoud, S. Ahmed, and I. Elarabawy, "Torque ripple reduction of radial magnetic gearbox using axial pole pairing," in *Proc. 7th IET Int. Conf. Power Electron., Mach. Drives (PEMD)*, Manchester, U.K., 2014, pp. 1–6.

[16] H. Zaytoon, A. S. Abdel-Khalik, S. Ahmed, and A. Massoud, "Cogging torque reduction of axial magnetic gearbox using pole pairing technique," in *Proc. IEEE Int. Conf. Ind. Technol. (ICIT)*, Seville, Spain, Mar. 2015, pp. 652–657.

[17] S. Gerber and R.-J. Wang, "Design and evaluation of a magnetically geared PM machine," *IEEE Trans. Magn.*, vol. 51, no. 8, Aug. 2015, Art. no. 8107010.

[18] P. M. Tlali, S. Gerber, and R.-J. Wang, "Optimal design of an outer-stator magnetically geared permanent magnet machine," *IEEE Trans. Magn.*, vol. 52, no. 2, Feb. 2016, Art. no. 8100610.

[19] X. Zhang, X. Liu, and Z. Chen, "Investigation of unbalanced magnetic force in magnetic geared machine using analytical methods," *IEEE Trans. Magn.*, vol. 52, no. 7, Jul. 2016, Art. no. 8104504.